WOOD RESEARCH **doi.org/10.37763/wr.1336-4561/71.3.437450**
e-ISSN 2729-8906
71(3): 2026 437-450 pp.

EXPERIMENTAL INVESTIGATION OF LOAD REDISTRIBUTION IN A HISTORIC-TYPE TIMBER ROOF SEGMENT UNDER PROGRESSIVE TIE-BEAM WEAKENING

JÁN BRODNIANSKY, SILVIA MARTINKOVIČOVÁ, JAROSLAV SANDANUS, TOMÁŠ KLAS
SLOVAK UNIVERSITY OF TECHNOLOGY IN BRATISLAVA
SLOVAK REPUBLIC

JIŘÍ KUNECKÝ, JIŘÍ BLÁHA, MICHAL KLOIBER
CZECH ACADEMY OF SCIENCES
CZECH REPUBLIC

(RECEIVED JUNE 2026)

ABSTRACT

This study examines how progressive loss of tie-beam stiffness redistributes deformation demand and internal force within an experimentally verified historic timber roof segment. A three-frame laboratory model was evaluated by close-range photogrammetry, inductive displacement sensing, post-test bending tests, and finite-element modelling. The measurements revealed clear frame-to-frame stiffness asymmetry, a distinct pre-cut settlement phase under sustained load, and accelerated deformation once the residual tie-beam section was substantially reduced. A refined model using member-specific elastic parameters reproduced the global loading response more accurately than a uniform-stiffness model. The damaged zone could also be represented by an equivalent rotational spring, although the fitted spring values remained response-dependent. The results indicate that lathing acted as a temporary redundancy path after severe weakening and that a nearly hinged residual section was not mechanically equivalent to a fully severed member within the tested configuration.

KEYWORDS: historic timber roof, progressive tie-beam weakening, load redistribution, equivalent rotational spring, lathing-based redundancy.

INTRODUCTION

Historic timber roofs are heterogeneous systems in which material variability, accumulated damage, hidden defects, workmanship irregularities, and repeated interventions influence structural response. Diagnosis of local damage is therefore challenging because even limited loss of cross-section may alter stiffness, internal force flow, and the stability reserve of

the whole roof segment (Yeomans 2003, Branco et al. 2014, Binda and Saisi 2005, Jasieńko et al. 2016, Ross 2015, Munafò et al. 2015, Zybała et al. 2022). Assessment should therefore address system-level redistribution mechanisms, rather than only isolated members (Stepinac et al. 2017, Nowak et al. 2013, Valipour et al. 2015).

Experimental research remains indispensable because it provides direct evidence on damaged timber systems and allows simplified analytical assumptions to be checked against measured response (Dinehart and Shenton 1998, Frese et al. 2012, Reynders et al. 2010, Neusch et al. 2022). Close-range photogrammetry and contact displacement sensing are especially suitable because they record both local discontinuities and global deformation patterns (Remondino 2011, Fassi et al. 2013, Luhmann et al. 2013, Mills et al. 2010, Özkan et al. 2022).

A still insufficiently quantified question concerns the role of secondary roof elements in emergency states. In historic roofs, battens or laths are often treated only as support for roof covering, although previous studies indicate that they may participate in longitudinal load transfer after local stiffness loss in a principal frame (Fragiacomo et al. 2011, Rug and Schober 2015, Valipour et al. 2015, Yang et al. 2020). Related work has also emphasized experimental verification, uncertainty-aware modelling, geometry reconstruction, and the sensitivity of timber response to joint stiffness and semi-rigid behaviour (Munafò et al. 2015, Neusch et al. 2022, Özkan et al. 2022, Zybała et al. 2022).

At the same time, quantitative evidence on how progressive local weakening of a tie beam alters the response of adjacent frames and the demand on the lathing-connected load path remains limited. This issue is especially relevant to localized decay, notching, and section loss in historic roofs, where member-specific stiffness differences, connection details, and the choice of reduced-order idealization may govern the actual redistribution mechanism (Brodniansky et al. 2026, Martinkovičová 2025a,b, Lyu et al. 2017, Liu and Xiong 2018).

This paper analyses a three-frame roof segment subjected to progressive weakening of the middle tie beam, focusing on measured response, member-specific model calibration, and reduced-order representation by an equivalent rotational spring. It asks whether optical and inductive measurements are consistent; how stiffness asymmetry, sustained loading, and cutting affect displacement histories; how well the refined model reproduces the response; and whether the damaged section can be represented by a practical equivalent rotational spring.

MATERIAL AND METHODS

Experimental dataset and evaluated stages

The analysed structure was a three-frame laboratory model of a historic timber roof segment connected by lathing. The test setup and selected observations are documented in the companion experimental paper (Brodniansky et al. 2026); the present study provides the quantitative and model-based interpretation. The principal Norway spruce (Picea abies (L.) H. Karst.) members were tie beams, rafters, and battens with nominal sizes of 60 × 80 mm, 40 × 60 mm, and 20 × 30 mm. The segment had one restrained support and one roller-type support. After stepwise loading and stabilization, the middle tie beam was progressively weakened by cutting 300 mm from the rafter-to-tie-beam connection.

The complete programme consisted of 27 measured states. For the present paper, the most relevant stages are the stabilized full-load state, the pre-cut full-load state after sustained

loading, the four intermediate cut depths, and the states after complete severing of the middle tie beam. Table 1 summarizes these stages for the loading, sustained-load, and damage analyses below. The final controlled collapse stage with additional external suspension was not used for calibration because the structural system had already been altered by the safety intervention.

Tab. 1: Measurement stages used for the detailed evaluation.

Stage	Elapsed time / reference	State description	Role in the present paper
14	full-load state	First complete ballast arrangement	Loading-phase reference for calibrated response
19	10,722 s after stage 14	Pre-cut full-load state	Reference state for damage evaluation and creep
20	after cut introduction	2 cm cut in middle tie beam	Initial weakening response
21	after further cutting	4 cm cut in middle tie beam	Intermediate weakening response
22	after further cutting	6 cm cut in middle tie beam	Advanced weakening response
23	after further cutting	7 cm cut in middle tie beam	Near-hinge response before full severing
24	post-severing phase	Complete severing of middle tie beam	Transition to hanging action
25	post-severing phase	State after full cut, before collapse	Post-severing comparison with numerical model
26	post-severing phase	Half-cut entrance tie beam; last self-supporting state	Limit state of temporary stability

Evaluation variables and reference states

The response was measured by close-range photogrammetry and six inductive displacement sensors. The comparison focused on the three tie-beam centres, where sensors I4V, I5V, and I6V corresponded to optical targets at the same structural locations (Fig. 1). Selected rafter points near the third lower batten were tracked on both sides of each frame; the original laboratory label "PC side" is retained only where needed for dataset traceability. Two optical points at the cut, ID_98 and ID_99, described the opening of the weakened section, with their positions at the 7 cm cut stage shown in Fig. 2.

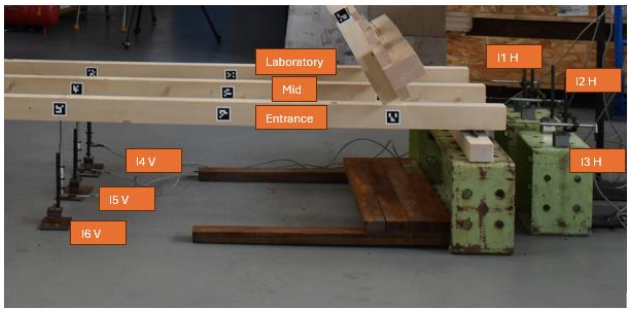

Fig. 1: Location of the vertical inductive displacement sensors on the three tie beams.

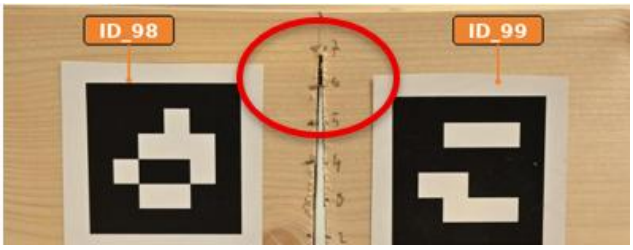

Fig. 2: Opening of the cut with optical targets ID_98 and ID_99 at the 7 cm cut stage.

Two reference states were used. For the global loading analysis, measurement No. 1, i.e. the unloaded model, served as the absolute zero state. For the damage phase, measurement

No. 19 was introduced as a local reference because it represented the stabilized full-load configuration immediately before cutting. This made it possible to separate the effect of progressive weakening from the preceding load-induced deflections. The sustained-load interval between measurements 14 and 19 lasted 10,722 s, i.e. 2 h 58 min 42 s. This interval was evaluated separately as a short-term creep or settlement phase. Measurement No. 27 was excluded from the quantitative comparison because the structure was already additionally suspended at the apex and no longer represented a purely self-supporting response.

Material testing and assignment of stiffness parameters

After the experiment, samples cut from battens, rafters, and tie beams were tested in bending. The dataset comprised 20 batten specimens (two from each of the 10 battens), 6 rafter specimens, and 3 tie-beam specimens. The bending arrangement followed STN EN 408+A1: 2013. For the tie beams, however, loading was limited to 15 kN and each specimen was tested in two orientations, resulting in six measurements on three physical specimens. The tests were used primarily to quantify member-specific stiffness differences rather than to classify the timber stock. The battens showed the highest stiffness and strength, with mean E = 15.2 GPa, 5% quantile of E = 11.0 GPa, and 5% bending strength = 69.7 MPa. The rafters had mean E = 12.5 GPa and 5% quantile of E = 9.0 GPa, but individual members ranged roughly from 9 to 14 GPa. The tie beams had the lowest mean stiffness, with mean E = 10.8 GPa and 5% quantile of E = 9.8 GPa. Within the model, the entrance tie beam was stiffer than the middle and laboratory tie beams. These experimentally derived values were used to assign member-specific elastic moduli to the refined numerical model (Tab. 2). The strength-class labels in the last column are used only as indicative stiffness-based equivalents linked to the adopted *E* values and should not be interpreted as formal grading results.

Tab. 2: Elastic parameters adopted for the refined numerical model.

Member / location	Assigned E [GPa]	Group mean E [GPa]	5% bending strength [MPa]	Indicative class by E
Tie beam - laboratory	10	10.8	-	C22
Rafter - laboratory, sliding-support side	9	12.5	57.5	C18
Rafter - laboratory, entrance side	14	12.5	57.5	C40
Tie beam - middle	10	10.8	-	C22
Rafter - middle, sliding-support side	14	12.5	57.5	C40
Rafter - middle, entrance side	9	12.5	57.5	C18
Tie beam - entrance	12	10.8	-	C30
Rafter - entrance, sliding-support side	14	12.5	57.5	C40
Rafter - entrance, entrance side	14	12.5	57.5	C40
Lathing	15	15.2	69.7	C45

Numerical models and calibration strategy

Two beam-type finite-element models were prepared in Dlubal RFEM with one-dimensional beam elements. The simplified model used a uniform C40-type timber stiffness and idealized supports; the refined model used the frame-specific elastic moduli from Tab. 2 and the actual restraint arrangement (Fig. 3). The geometry reproduced the three measured

frames, batten levels, and asymmetric support concept. Lathing was modelled by beam members connected to the rafters at the batten levels, and the reported idealized nail axial force denotes the force in the most loaded batten-to-rafter link. Local slip and withdrawal were not modelled explicitly. When the cut was represented directly, the weakened section was introduced as a short member segment with reduced section properties.

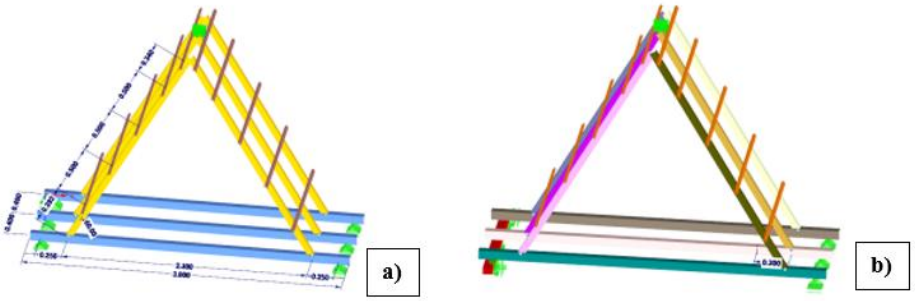

Fig. 3: Simplified and refined FE models used in the calibration and redistribution analyses.

During the loading phase, the vertical displacements at the three tie-beam midspans were selected as the primary calibration targets because they were measured by both monitoring systems and provided a representative measure of global frame stiffness. Model performance was evaluated mainly by mean absolute error (MAE = (1/n) Σ |u_exp,i - u_num,i|). Fig. 4 compares the measured and numerical tie-beam histories, while rafter displacements were treated only as secondary comparison quantities. Damage-phase results were subsequently used to assess the predictive consistency of the calibrated global model rather than to re-identify its parameters. Because both phases were obtained from the same specimen, the damage-phase comparison should not be interpreted as independent statistical validation.

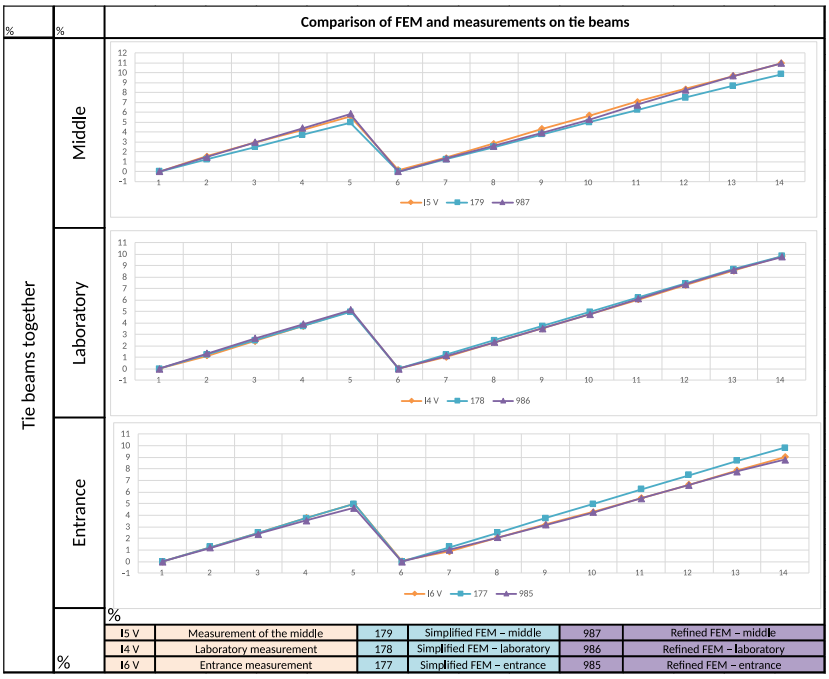

Fig. 4: Comparison of experimental and numerical tie-beam midspan displacements; x-axis = measurement number, y-axis = displacement [mm].

For the damage phase, the cut was represented either by a locally weakened beam segment or by an equivalent rotational spring. The spring is treated here as a response-based reduced-

order representation of local flexural compliance, not as a transferable material parameter. Two definitions were retained: k1 reproduces the experimentally measured local cut-opening response, whereas k2 reproduces the refined numerical model with explicit weakening. The parameters therefore have different calibration targets and should not be treated as interchangeable.

RESULTS AND DISCUSSION

Consistency of optical and inductive measurements

The optical and inductive measurements showed good agreement in the deformation range relevant to the loading phase. In the representative pre-cut full-load state, the differences between the sensor readings and the corresponding optical points at the three tie-beam midspans remained below about 0.35 mm. These results indicate that both systems captured the global displacement response consistently and support the use of optical measurements at locations without contact sensors.

Comparison of the rafter measurements led to the same qualitative conclusion, although with greater scatter. The differences were mainly associated with the optical visibility conditions of individual targets. Points partially obscured by neighbouring members or located deeper along the viewing direction of the entrance-side camera exhibited less stable measurement histories than clearly exposed points. Even in these cases, however, the overall loading trend and the ranking of the frames remained consistent.

The horizontal measurements indicated that no significant global sway developed during loading. The maximum measured horizontal displacement was approximately 1 mm at the highest load level, indicating that the measured vertical displacements predominantly reflected the stiffness of the roof segment itself and not rigid-body motion of the entire setup.

Loading-phase response and frame-to-frame stiffness asymmetry

The loading phase demonstrated clear differences in stiffness among the three transverse frames. At the first full-load state, tie-beam midspan deflections were 9.831 mm for the laboratory frame, 10.969 mm for the middle frame, and 9.019 mm for the entrance frame. The middle frame exhibited the greatest deformation, whereas the entrance frame exhibited the smallest deformation, consistent with its stiffer tie beam and relatively stiff rafters.

The rafter histories confirmed this non-uniformity (Figs. 5 and 6). Fig. 5 summarizes the response on the sliding-support side, whereas Fig. 6 summarizes the entrance-side response at the restrained support. At the full-load state, on the entrance side, the laboratory and middle rafters reached 14.404 mm and 12.743 mm, while the corresponding sliding-support-side rafters reached only 9.809 mm and 10.632 mm. This behaviour is consistent with the material tests, which identified rafter subgroups with elastic moduli of approximately 9 and 14 GPa. The tie-beam calibration values are compiled in Tab. 3.

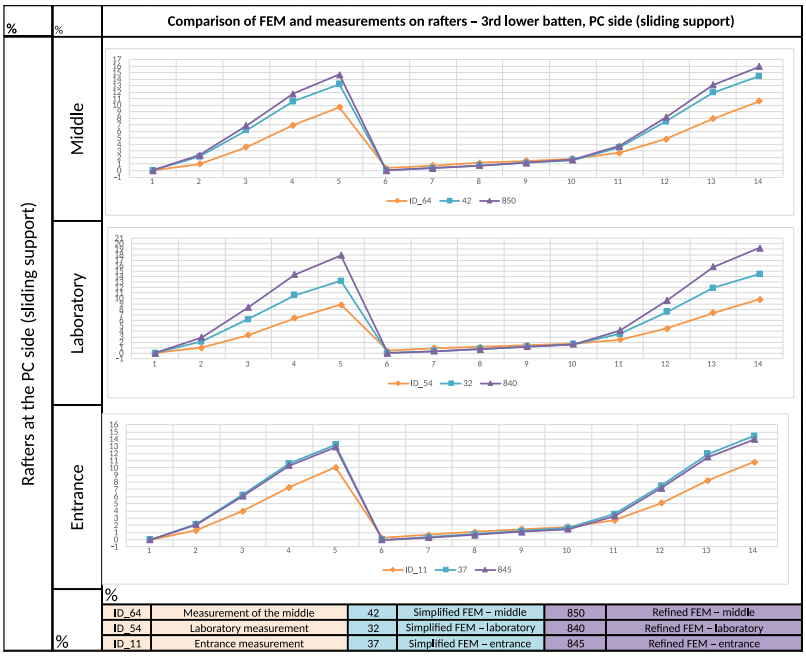

Fig. 5: Comparison of FEM results and measured rafter displacements at the third lower batten on the sliding-support side [mm].

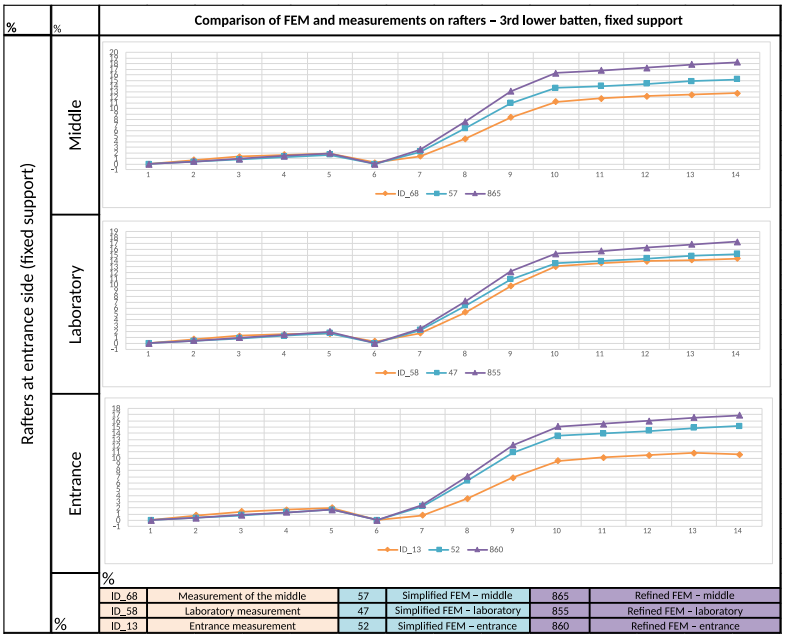

Fig. 6: Comparison of FEM results and measured rafter displacements at the third lower batten on the entrance side (restrained support) [mm].

Tab. 3: Tie-beam midspan deflections at the first full-load state (stage 14)

Frame	Experiment [mm]	Simplified model [mm]	Refined model [mm]	Abs. error, simplified [mm]	Abs. error, refined [mm]
Laboratory	9.831	9.817	9.742	0.014	0.089
Middle	10.969	9.817	10.970	1.152	0.001
Entrance	9.019	9.817	8.770	0.798	0.249

Tab. 3 demonstrates the influence of stiffness heterogeneity on the model response. At the stage-14 full-load state, the simplified model reproduced the average level of tie-beam

deflection but did not reproduce the experimentally observed differences among the three frames. The refined model reproduced the relative stiffness ranking of the three frames and reduced the mean absolute error across the three tie-beam midspans, indicating that member-specific elastic parameters improved the representation of the measured stiffness asymmetry.

Sustained-load response at full ballast

The interval between measurements 14 and 19 captured the short-term time-dependent response under constant full load. During the 10,722 s interval, additional tie-beam deflection was 0.563 mm for the laboratory frame, 0.669 mm for the middle frame, and 0.487 mm for the entrance frame. Although relatively small, these systematic increments justify using measurement No. 19 as the reference state for evaluating the subsequent damage response.

Using this reference state separates the deformation accumulated during sustained loading from the subsequent deformation associated with progressive weakening. By referencing the cut phase to measurement No. 19, the interpretation remains limited to the structural consequences of the progressive loss of tie-beam stiffness.

Measured redistribution during progressive weakening

The measured displacement histories during progressive cutting, summarized in Tab. 4, indicate three distinct response stages. The first stage, up to a cut depth of 4 cm, is characterized by only moderate increases in the displacements of the adjacent intact frames. The second stage, between the 4 cm and 6 cm cuts, is marked by a rapid acceleration of the response near the damaged section. The third stage, represented by the 7 cm cut and subsequent complete severing, corresponds to the transition from a weakened but continuous frame to a post-severing configuration in which load was redistributed through the lathing-connected system.

Tab. 4: Measured displacements during progressive cutting of the middle tie beam

Cut depth [cm]	Tie beam, laboratory [mm]	Tie beam, middle [mm]	Tie beam, entrance [mm]	Cut point ID_98 [mm]	Cut point ID_99 [mm]
0	10.394	11.638	9.506	7.092	7.809
2	10.550	11.769	9.600	7.484	8.219
4	10.769	12.363	9.825	9.153	9.989
6	11.875	15.613	10.831	15.691	16.963
7	12.788	18.900	11.638	21.539	23.040

Tab. 4 shows that the damaged middle tie beam reacted much more strongly than the two intact edge frames. Relative to the pre-cut state, its deflection increased by 0.131 mm at the 2 cm cut, 0.725 mm at the 4 cm cut, 3.975 mm at the 6 cm cut, and 7.262 mm at the 7 cm cut. Over the same interval, the neighbouring tie beams increased by only about 2.39 mm and 2.13 mm. Redistribution was therefore detectable at small cut depths, but its decisive acceleration occurred only after strong section loss.

The two points located directly at the cut, ID_98 and ID_99, documented the local opening very clearly. Fig. 2 shows the geometry of this opening at the last pre-severing stage, while Tab. 4 summarizes the measured increments. Relative to the pre-cut state, their displacements increased by about 0.4 mm at the 2 cm cut, about 2.1 mm at the 4 cm cut, about 8.6-9.2 mm at the 6 cm cut, and about 14.4-15.2 mm at the 7 cm cut. The monotonic increase supports the interpretation of a progressively opening rotational discontinuity.

After complete severing of the middle tie beam, the response changed abruptly. Relative to measurement No. 19, the middle tie beam increased by about 44.7 mm, while the laboratory and entrance tie beams increased by only about 5.3 mm and 4.8 mm in the post-cut state before collapse. The specimen therefore did not lose stability immediately; instead, the middle frame entered a temporary hanging mechanism in which the load was transferred longitudinally through the lathing to the adjacent intact frames.

Material properties and their structural meaning

The material tests explain why the experimentally observed response was non-uniform from the beginning. The entrance tie beam was stiffer than the other two tie beams, and the rafters were distributed between markedly softer and markedly stiffer subgroups. The battens, by contrast, combined the highest stiffness with high dimensional precision. Structurally, this means that non-identical principal frames were linked by a relatively strong and stiff longitudinal connecting system, which naturally favoured redistribution through the battens once one frame lost stiffness.

These tests provide independent evidence that member-to-member stiffness variability contributed to the measured structural asymmetry and support the use of member-specific material properties in the numerical model.

Calibration of the numerical model

The loading phase was used to calibrate the numerical model prior to the progressive-cutting experiment. The tie-beam midspans were selected as the primary calibration targets because they provided the clearest and most stable measures of global frame stiffness. At stage 14, the simplified model reproduced only the average level of tie-beam deflection and therefore failed to capture the experimentally observed asymmetry. The refined model reproduced the relative stiffness of the three frames and substantially reduced the tie-beam midspan displacement errors compared with the uniform-stiffness model.

The comparison of rafter displacements was less consistent. Although the refined model preserved the frame-to-frame stiffness differences from the material tests, it did not improve every individual rafter history. Some rafter targets were more sensitive to visibility, local connection effects, and support-detail idealization than the tie-beam centres. The rafter traces are therefore treated as a secondary comparison quantity rather than the dominant calibration target.

The calibrated refined model should therefore be interpreted primarily as a model of global structural response during loading and progressive weakening. It provides a mechanically plausible basis for internal-force redistribution, but not a fully resolved description of every connection detail. At advanced damage stages, where connection slip and geometric discontinuities may become increasingly important, greater differences between numerical and experimental responses should be expected.

Rotational-spring representation of the cut

Explicit section reduction reproduced the early stages of cutting reasonably well but underestimated the flexibility of the damaged region at larger cut depths. The equivalent rotational spring was therefore introduced as a response-based reduced-order representation of

local stiffness loss, not as a uniquely identifiable physical property. Comparable spring-type idealizations have been adopted when full local modelling is impractical (Liu and Xiong 2018).

Accordingly, k1 is calibrated to the measured local cut-opening response, whereas k2 is calibrated to the explicit weakened-section model. The resulting values are listed in Tab. 5.

Tab. 5: Equivalent rotational spring stiffness of the cut

Cut depth [cm]	Spring stiffness k1 experiment-based [kNm/rad]	Spring stiffness k2 numerical-reference [kNm/rad]
2	200	700
4	34	400
6	2.5	5.1
7	0.001	2.4

The results in Tab. 5 indicate strongly non-linear degradation of the local rotational stiffness. Both stiffness curves show that the cut remained relatively stiff at 2 cm and 4 cm, whereas a pronounced drop occurred between 4 cm and 6 cm. At a cut depth of 7 cm, the identified spring stiffness approached a near-hinge kinematic condition, confirming that the decisive loss of rotational restraint occurred only after substantial reduction of the residual section.

The difference between k1 and k2 is methodologically important. Parameter k1 includes measurement scatter, local contact effects, and stiffness contributions only partly captured by the beam idealization, whereas k2 preserves consistency within the explicit numerical model. The spring representation should therefore be interpreted as a compact, configuration-specific reduced-order description of local stiffness loss. This target dependence is consistent with response-based stiffness-identification procedures (Lyu et al. 2017, Liu and Xiong 2018).

In the present paper, the main value of the spring idealization lies in its ability to distinguish between moderately weakened, near-hinge, and fully severed states within the global response of the roof segment. A more formal response-based procedure for weakening acting over finite lengths is outside the scope of the present paper.

Internal force redistribution and lathing demand

The refined numerical model provides a mechanically plausible interpretation of the measured redistribution. The corresponding response indicators are listed in Tab. 6. With increasing cut depth, the calculated axial force in the middle tie beam changed from tension to compression, while that in the adjacent rafter changed from compression to tension. This behaviour indicates a gradual shift in the calculated load-transfer mechanism of the damaged frame from ordinary frame action toward a configuration supported by the longitudinal connecting system.

Tab. 6 shows that calculated normal stress in the lathing increased with cut depth and peaked after complete severing of the middle tie beam. The values remained below those suggested by the batten bending tests, but this is only an indicative plausibility check because numerical stress output and laboratory strength do not represent identical limit states. The result nevertheless supports the observed temporary survival of the damaged frame.

Tab. 6: Selected numerical response quantities during weakening of the middle frame (positive axial force = tension; negative = compression).

State	Tie-beam axial force [kN]	Lath normal stress [MPa]	Idealized nail axial force [kN]	Adjacent rafter axial force [kN]
0 cm cut	0.28	3.92	-0.02	-1.25
2 cm cut	0.25	4.30	-0.02	-1.19
4 cm cut	0.14	5.94	-0.01	-0.95
6 cm cut	-0.35	16.35	0.04	0.23
7 cm cut	-0.58	22.14	0.06	0.71
Full cut	0.00	48.98	0.48	0.20

The results also show that a near-perfect hinge and a completely severed member are not equivalent for the secondary load path. At the 7 cm cut, the battens were heavily engaged, and the lath stress was about 22 MPa; after complete severing, the normal stress in the most heavily loaded batten reached approximately 49 MPa. Thus, residual tie-beam continuity remained structurally relevant even when the damaged section approached a near-hinge kinematic condition. The calculated idealized nail force provides additional numerical support for this interpretation. It denotes the axial force at the most critical idealized batten-to-rafter link, not an explicitly resolved fastener response. The force was negligible in intact and moderately weakened states but increased sharply after complete severing, reaching the same order as a design back-calculation for a 2.5 × 60 mm nail. Together with the observed partial withdrawal, these results are consistent with published findings on nailed timber joints (Moya and Tenorio 2017) and indicate that batten connections formed part of the temporary load-transfer mechanism.

Implications for the assessment of historic roofs

Two broader implications can be identified for the assessment of historic timber roofs. First, battens or comparable secondary members should be considered in models used to assess localized damage, because they may temporarily act as redundancy elements after stiffness loss in one principal frame. This interpretation is broadly consistent with earlier studies on load redistribution in timber systems and with assessment-oriented work on historic roofs (Fragiacomo et al. 2011, Valipour et al. 2015, Munafò et al. 2015, Zybała et al. 2022). Compared with these more general studies, the present experiment adds direct evidence from an instrumented historic roof-segment configuration in which redistribution developed through an explicitly modelled lathing-connected path. It also agrees with Wood Research studies showing that secondary stiffening elements and semi-rigid timber connections can influence global timber response more strongly than simplified member-by-member assessment would suggest (Yang et al. 2020, Neusch et al. 2022). Second, the modelling strategy should distinguish clearly between a severely weakened but still continuous member and a completely severed member. For the global kinematics of the main frame, both states may appear similar, yet for the demand on the lathing and its connections the difference is substantial.

The experiment also illustrates why calibration against measured displacements is essential. A model with uniform material parameters can reproduce the average displacement level, but member-specific stiffness differences were needed to make the measured redistribution mechanically consistent. In this sense, the present study complements broader

survey-and-modelling workflows by showing which response features must be captured if a structural model is to support diagnostic interpretation (Mills et al. 2010, Özkan et al. 2022).

CONCLUSIONS

The combined optical and inductive monitoring provided sufficiently consistent displacement data for quantitative interpretation. Agreement was strongest at the tie-beam midspans, whereas the somewhat larger scatter at selected rafter points was attributable mainly to optical visibility conditions and local effects.

The measured loading histories showed that the three transverse frames were not equally stiff and that the stabilized pre-cut full-load state was the appropriate local reference for evaluating the damage phase. Progressive cutting initially caused limited redistribution, followed by a rapid increase in local compliance after substantial section loss. After complete severing, the damaged frame developed a temporary post-severing load-transfer configuration involving the adjacent frames and the lathing.

A refined numerical model based on member-specific elastic properties reproduced the global loading response more accurately than a uniform-stiffness model. The equivalent rotational-spring formulation provided a useful reduced-order representation of local stiffness loss, although the fitted spring values remained response-dependent and should therefore be interpreted as response-based surrogate parameters rather than transferable physical properties.

The experimental and numerical results indicate that the lathing became an increasingly important component of the temporary longitudinal load-transfer mechanism, particularly after complete severing of the middle tie beam. A severely weakened but still continuous tie beam is therefore not mechanically equivalent to a fully severed member when the demand on secondary elements and their connections is assessed. This distinction is relevant to the assessment of historic timber roofs and to the development of reduced numerical models for localized damage.

The findings are limited to the tested roof segment, structural configuration, and damage location, as well as to a beam-type idealization of the members and connections that did not explicitly represent connection slip or withdrawal. Because only one roof segment was tested, the quantitative comparisons are descriptive, and no inferential statistical generalization is claimed. The present calibration did not include a formal probabilistic uncertainty or parameter-sensitivity analysis. The reported spring stiffnesses and connection-level force indicators should therefore be regarded as configuration-specific, response-based quantities rather than transferable physical properties.

ACKNOWLEDGMENTS

The research was supported by the project “Wooden structures prevention and maintenance for heritage conservation purposes” (NAKI III, reg. No. DH23P03OVV005), provided by the Ministry of Culture of the Czech Republic.

REFERENCES

1. Binda, L., Saisi, A., 2005: Investigation strategies for the diagnosis of historic structures. Construction and Building Materials 19(8): 609-619.
2. Branco, J.M., Cruz, P.J.S., Piazza, M., 2014: Assessment, diagnosis and strengthening of timber structures. Construction and Building Materials 58: 1-13.
3. Brodniansky, J., Martinkovičová, S., Sandanus, J., Klas, T., Kunecký, J., Bláha, J., Kloiber, M., 2026: The experimental investigation of a model of a historical-type timber roof segment under progressive tie-beam weakening. Wood Research 71(2).
4. Dinehart, D.W., Shenton, H.W., 1998: Experimental testing of timber trusses. Journal of Structural Engineering 124(2): 123-130.
5. EN 408 +A1, 2013: Timber structures. Structural timber and glued laminated timber. Determination of some physical and mechanical properties.
6. Fassi, F., Achille, C., Fregonese, L., Adami, A., 2013: Photogrammetry for structural monitoring. ISPRS Annals of the Photogrammetry, Remote Sensing and Spatial Information Sciences II-5/W1: 115-122.
7. Fragiacomo, M., Amadio, C., Macorini, L., 2011: Load distribution in timber structures. Engineering Structures 33(2): 399-407.
8. Frese, M., Blass, H.J., Schädle, P., 2012: Full-scale testing of timber structures. Engineering Structures 40: 457-466.
9. Jasieńko, J., Nowak, T., Bednarz, Ł., 2016: Failure analysis of historical timber structures. Materials and Structures 49: 123-134.
10. Liu, Y., Xiong, H., 2018: Lateral performance of a semi-rigid timber frame structure: theoretical analysis and experimental study. Journal of Wood Science 64: 591-600.
11. Lyu, M., Zhu, X., Yang, Q., 2017: Connection stiffness identification of historic timber buildings using temperature-based sensitivity analysis. Engineering Structures 131: 180-191.
12. Luhmann, T., Robson, S., Kyle, S., Harley, I., 2013: Close-range photogrammetry and 3D imaging. 2nd ed. De Gruyter. Pp. 684.
13. Martinkovičová, S., 2025a: Vybrané problémy modelovania historických krovov (Selected issues in the modelling of historical roof trusses). Doctoral thesis (in Slovak). Slovak University of Technology in Bratislava, Faculty of Civil Engineering, Bratislava. Pp. 124. https://opac.crzp.sk/?fn=detailBiblioForm&sid=BA75C2D62745AD5722E4929ED92F
14. Martinkovičová, S., Sandanus, J., Brodniansky, J., Ondrašinová, L., 2025b: Static analysis of selected types of roof trusses considering the weakening of the structural elements. Slovak Journal of Civil Engineering 33(3): 47-53.
15. Mills, J., Barber, D., Bryan, P., 2010: Metric survey for structural analysis of historic buildings. Journal of Architectural Conservation 16(3): 7-22.
16. Moya, R., Tenorio, C., 2017: Strength and displacement under tension and compression of wood joints fastened with nails and screws for use in trusses in Costa Rica. Wood Research 62(1): 139-156.
17. Munafò, P., Stazi, F., Tassi, C., Davì, F., 2015: Experimentation on historic timber trusses to identify repair techniques compliant with the original structural-constructive conception. Construction and Building Materials 87: 54-66.

18. Neusch, M., Sandanus, J., Freudenberger, K., 2022: Experimental verification of the modern semi-rigid timber connections. Wood Research 67(6): 1005-1016.
19. Nowak, T., Jasieńko, J., Bednarz, Ł., 2013: Failure mechanisms of timber roof trusses. Engineering Structures 52: 1-10.
20. Özkan, T., Pfeifer, N., Styhler-Aydın, G., Hochreiner, G., Herbig, U., Döring-Williams, M., 2022: Historic timber roof structure reconstruction through automated analysis of point clouds. Journal of Imaging 8(1): 10.
21. Remondino, F., 2011: Heritage recording and 3D modeling with photogrammetry. Remote Sensing 3(6): 1104-1138.
22. Reynders, E., Wursten, G., De Roeck, G., 2010: Structural health monitoring of civil engineering structures. Mechanical Systems and Signal Processing 24(3): 611-626.
23. Ross, R.J., 2015: Nondestructive evaluation of wood. 2nd ed. Forest Products Laboratory, USDA.
24. Rug, W., Schober, K.U., 2015: Load-bearing behaviour of timber trusses. Construction and Building Materials 76: 360-368.
25. Stepinac, M., Rajčić, V., Barbalić, J., 2017: Behaviour of timber structures under damage conditions. Engineering Structures 148: 62-74.
26. Valipour, H.R., Bradford, M.A., Gilbert, R.I., 2015: Load redistribution in timber structures after element failure. Construction and Building Materials 76: 412-422.
27. Yang, X., Zhao, Q., Hao, D., Wang, J., Fu, S., Ma, L., 2020: Flexural behavior of OSB reinforced wood truss. Wood Research 65(2): 245-256.
28. Yeomans, D., 2003: The repair of historic timber structures. Thomas Telford.
29. Zybała, T., Szepietowska, K., Bukal, G., Lubowiecka, I., 2022: Portico Farmhouses of the Vistula Delta: Architecture, Current State and Finite Element Modelling of Timber Roof Truss under Material and Cross-section Uncertainty. International Journal of Architectural Heritage 16(12): 1885-1906.

JÁN BRODNIANSKY*, SILVIA MARTINKOVIČOVÁ, JAROSLAV SANDANUS,
TOMÁŠ KLAS
SLOVAK UNIVERSITY OF TECHNOLOGY IN BRATISLAVA
DEPARTMENT OF STEEL AND TIMBER STRUCTURES
RADLINSKÉHO 11, 810 05 BRATISLAVA, SLOVAK REPUBLIC
*Corresponding author: jan_brodniansky@stuba.sk

JIŘÍ KUNECKÝ, JIŘÍ BLÁHA, MICHAL KLOIBER
CZECH ACADEMY OF SCIENCES
INSTITUTE OF THEORETICAL AND APPLIED MECHANICS
PROSECKÁ 809/76, 190 00 PRAGUE 9
CZECH REPUBLIC